Supplementary Information

Unveiling Wavelength-Dependent Light Roles on Dynamic Structures for Photothermal Toluene Oxidation over Atomically Dispersed Pd/TiO_2

Xin Wang,[a] Maosen Xu,[a] Jinhua Feng,[a] Deyun Ma,[b] Weiping Zhang,[a] Meicheng Wen,[a] Hongli Liu[a]*

[a] Guangdong Key Laboratory of Environmental Catalysis and Health Risk Control, Guangdong Engineering Technology Research Center for Photocatalytic Technology Integration and Equipment, Institute of Environmental Health and Pollution control, Guangdong University of Technology, Guangzhou 510006, China.

[b] School of Food and Pharmaceutical Engineering, Zhaoqing University, Zhaoqing 526061, China

*** Corresponding author**: Prof. Hongli Liu, E-mail: liuhl@gdut.edu.cn

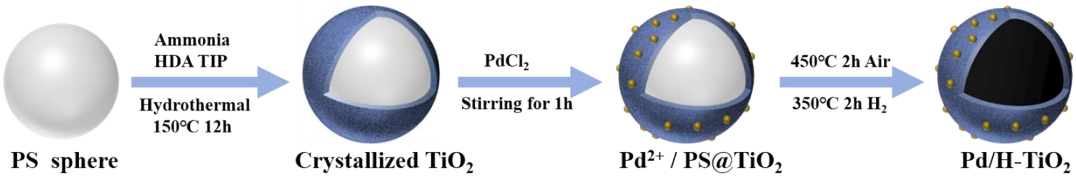

Figure S1. Schematic preparation of Pd/H-TiO_2.

Pd/H-TiO_2 were synthesized by *in situ* growth of TiO_2 on the surface of PS spheres, followed by the introduction of varying amounts of Pd and subsequent template removal through calcination. The as-obtained samples were denoted as X% Pd/H-TiO_2 (X = 1, 1.5 and 2) and the actual content of Pd in these samples was 1.07, 1.51 and 1.88 % determined by atomic absorption spectrometry (AAS).

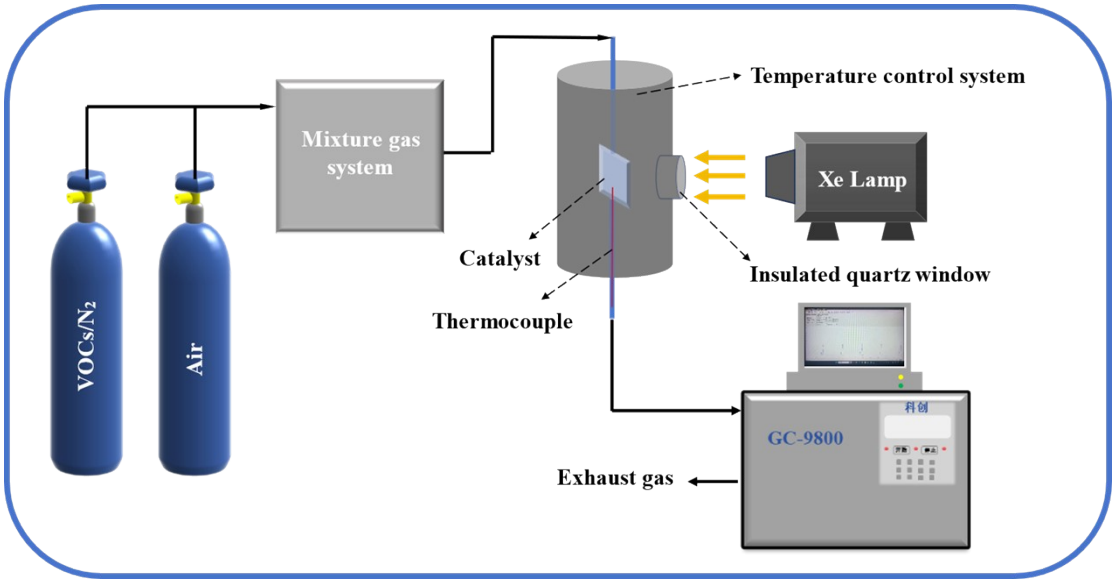

Figure S2. Diagram of photothermal synergistic catalytic oxidation device.

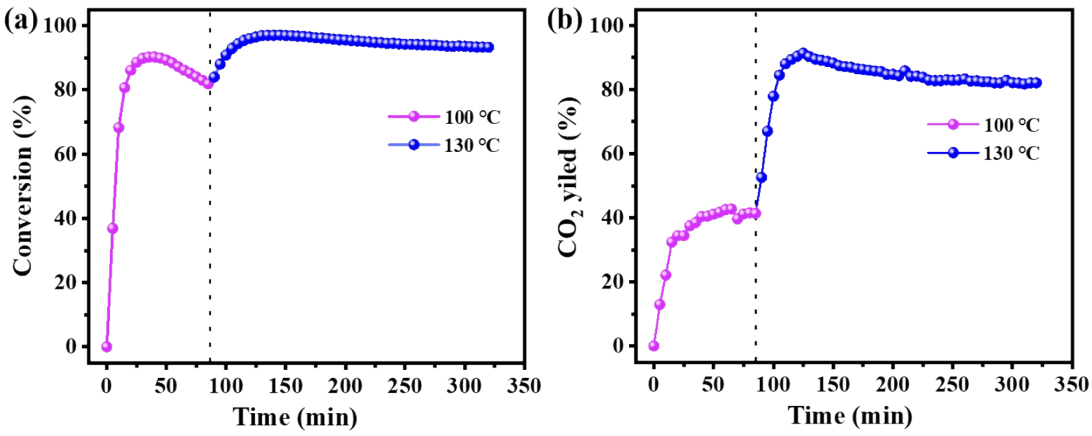

Figure S3. (a) Toluene conversion and (b) CO_2 yield over 1.5% Pd/H-TiO_2 under UV-Vis light at 100 and 130 ℃.

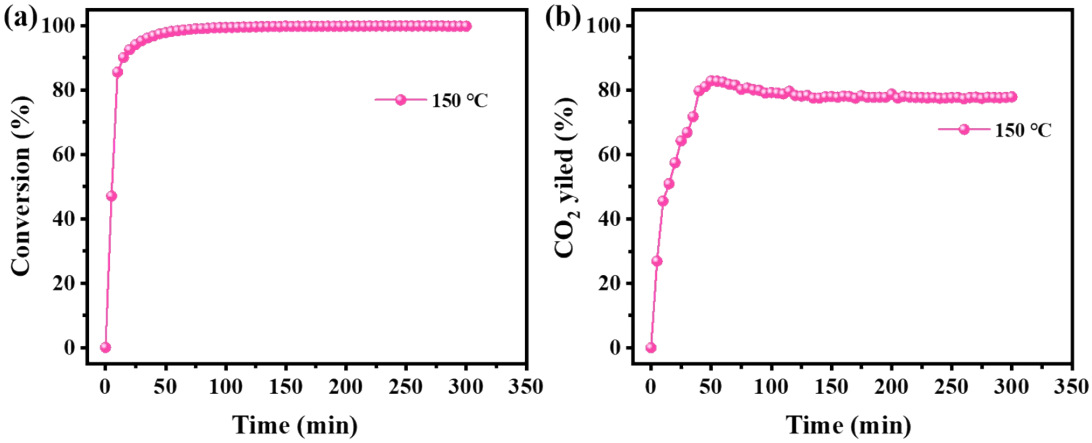

Figure S4. (a) Toluene conversion and (b) CO_2 yield over 1.5% Pd/H-TiO_2 under UV-Vis light at 150 ℃.

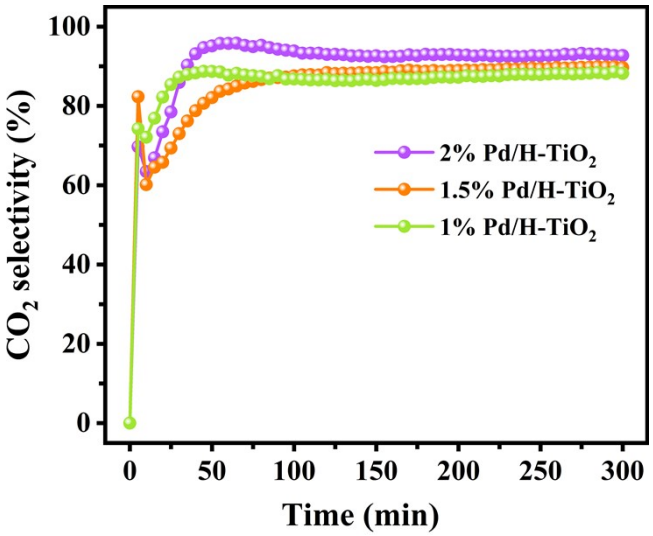

Figure S5. CO_2 selectivity of Pd/H-TiO_2 under UV-Vis light at 130 ℃.

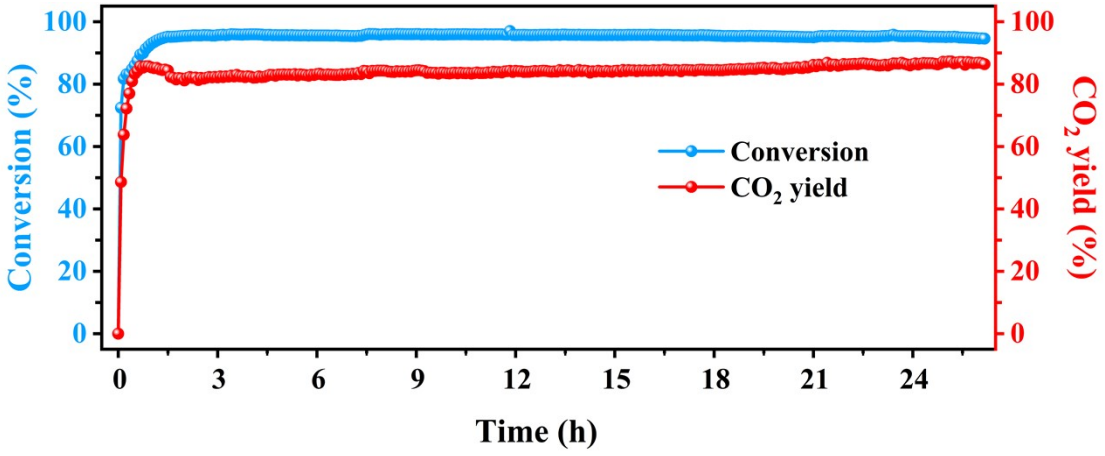

Figure S6. Photothermal catalytic stability test over Pd/H-TiO_2 under UV-Vis light at 130 ℃.

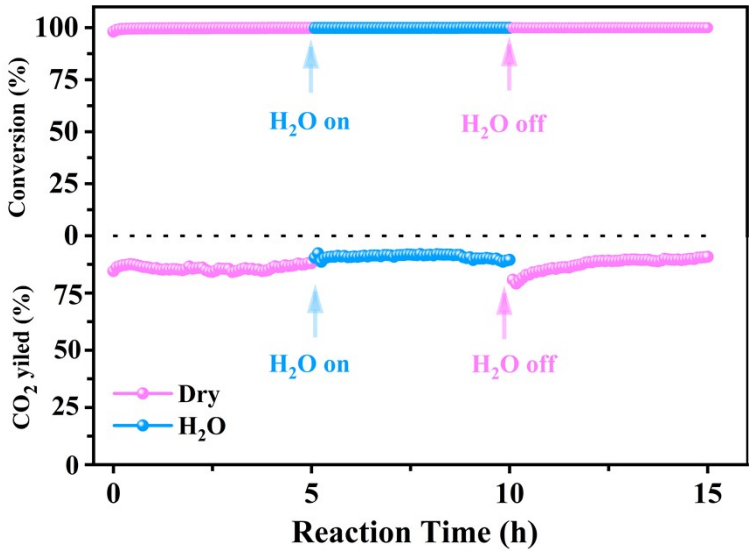

Figure S7. Photothermal catalytic activity for toluene oxidation over Pd/H-TiO_2 under humidity under UV-Vis light at 130 ℃.

It is highly desirable for a catalyst to exhibit excellent stability and water resistance to ensure its suitability for practical applications. The stability of the Pd/H-TiO_2 catalyst was evaluated under UV-Vis light at 130 °C. As shown in Figure S6, the Pd/H-TiO_2 demonstrated remarkable stability during 25 h of toluene oxidation (dry conditions), maintaining a toluene conversion of 94.5% and a CO_2 yield of 86.3%. In practical industrial applications, water vapor is often present. To evaluate the catalyst's water resistance, 10 vol% water vapor was introduced after 5 hours of catalytic reaction. As shown in Figure S7, following the introduction of water vapor, the toluene conversion remained stable. Surprisingly, the CO_2 yield increased from an average of 85.9% to 90.9%. After the water vapor was removed, the CO_2 yield stabilized at 90.7%.

According to previous study, the oxygen in the water would exchange with the adsorbed oxygen or lattice oxygen of the catalyst, generating new OOH species, which could be decomposed into •OH.[1] The •OH could further react with the adsorbed oxygen, generating more active oxygen species ($•O_2^-$ and $•O^-$).[2] Therefore, the improved catalytic activity after the introduction of water was reasonable. The above results indicate that Pd/H-TiO_2 exhibits excellent stability and water resistance, demonstrating its practical applicability in the photothermal degradation of toluene.

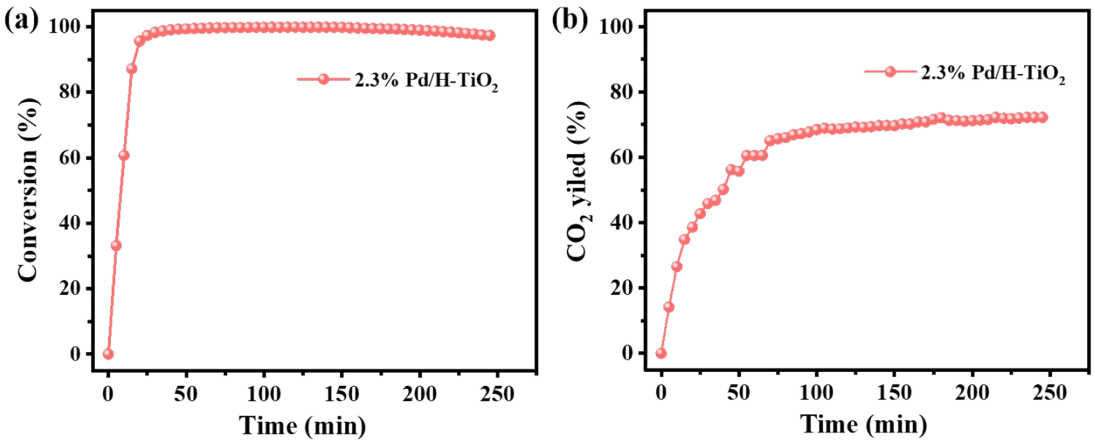

Figure S8. (a) Toluene conversion and (b) CO_2 yield over 2.3% Pd/H-TiO_2 under UV-Vis light at 130 ℃.

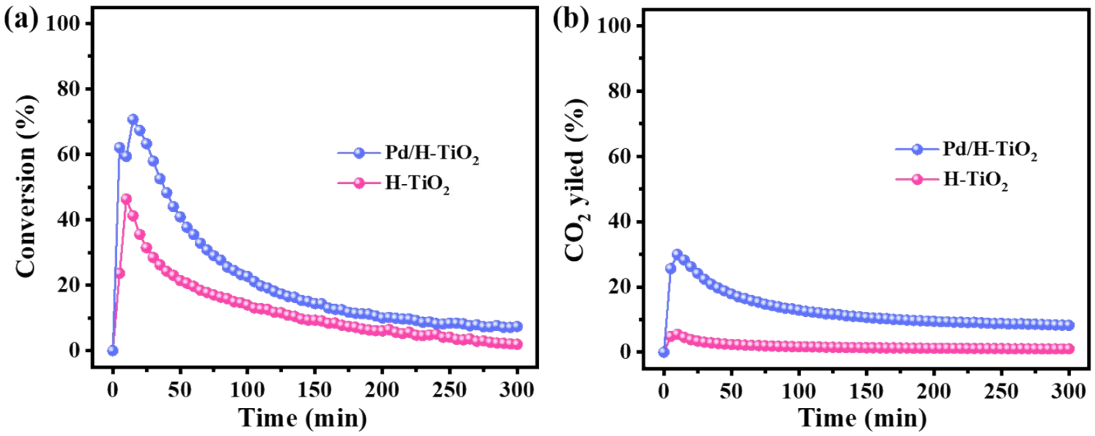

Figure S9. (a) Toluene conversion and (b) CO_2 yield over H-TiO_2 and Pd/H-TiO_2 under UV-Vis light at 30 ℃.

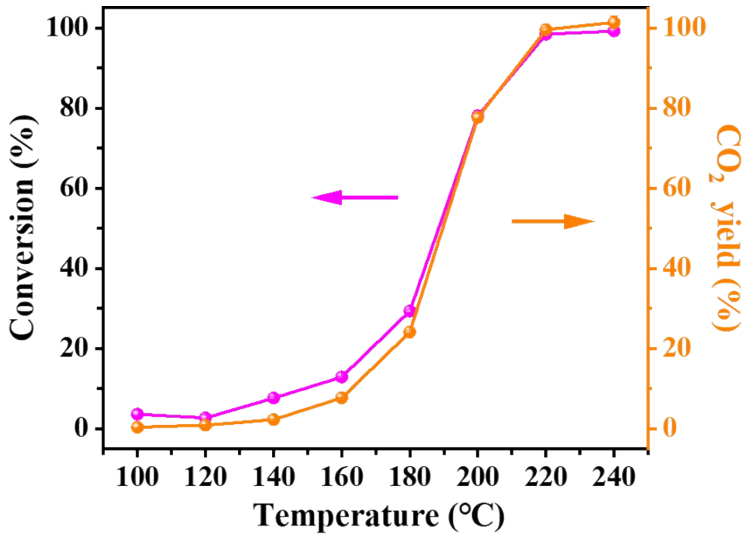

Figure S10. Toluene conversion and CO_2 yield over Pd/H-TiO_2 under different reaction temperatures without light irradiation.

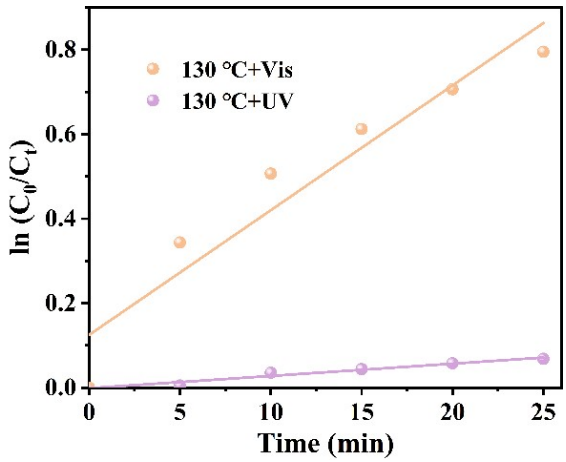

Figure S11. Pseudo first-order kinetic fitting curves of CO_2 yield

The CO_2 yield over Pd/H-TiO_2 under UV and visible light irradiation was also evaluated using a pseudo-first-order kinetic model. The apparent reaction rate constants (k) can be evaluated from the slope of $\ln(C_0/C_t)$ versus time curves (Figure 11). Based on this analysis, the k values under UV and visible photothermal catalytic conditions were determined to be 2.9×10^{-3} and 29.5×10^{-3} min^{-1}, respectively (Table S2). Clearly, the k value under visible-light conditions is about ten times higher than that under UV irradiation, which provides quantitative support for the distinct reaction behaviors and pathways induced by different irradiation wavelengths.

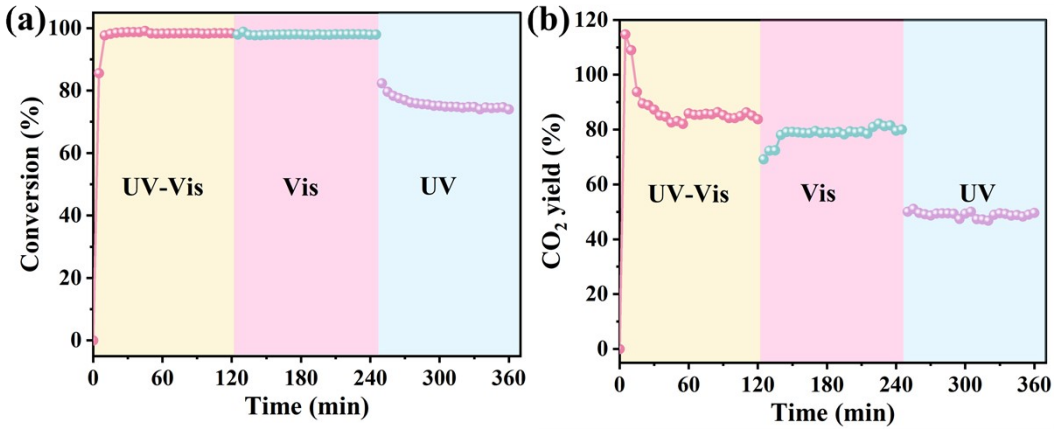

Figure S12. (a) DCM conversion and (d) CO_2 yield over Pd/H-TiO_2 under photothermal catalysis with different light irradiation.

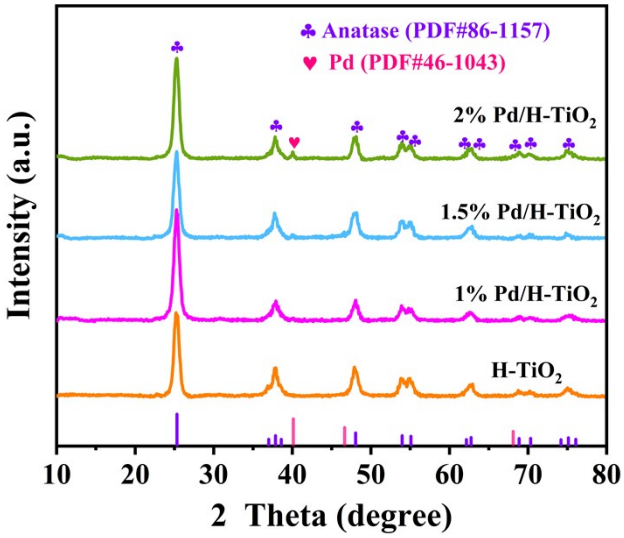

Figure S13. XRD patterns of the H-TiO_2 and Pd/H-TiO_2 samples.

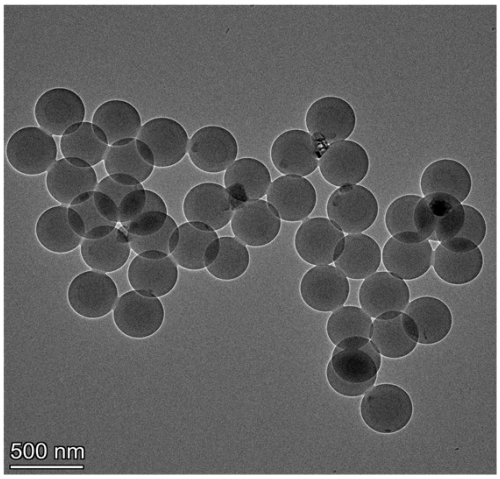

Figure S14. TEM images of polystyrene spheres.

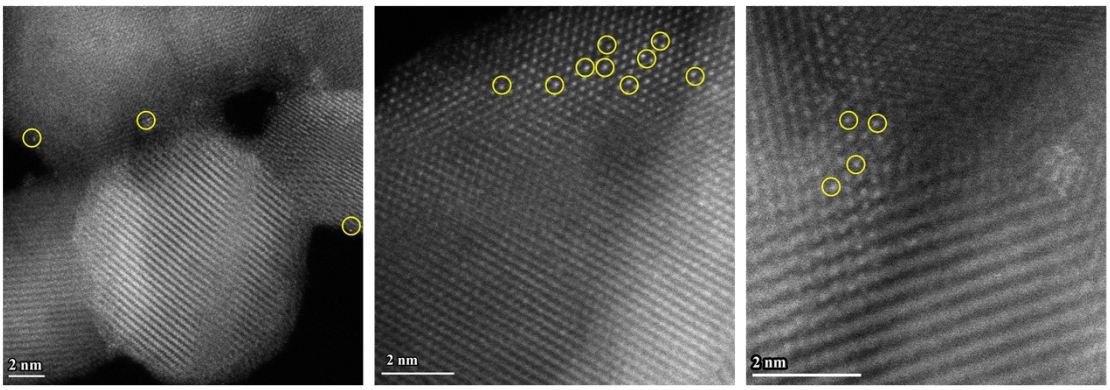

Figure S15. AC-HAADF-STEM images of the 2% Pd/H-TiO_2 catalyst.

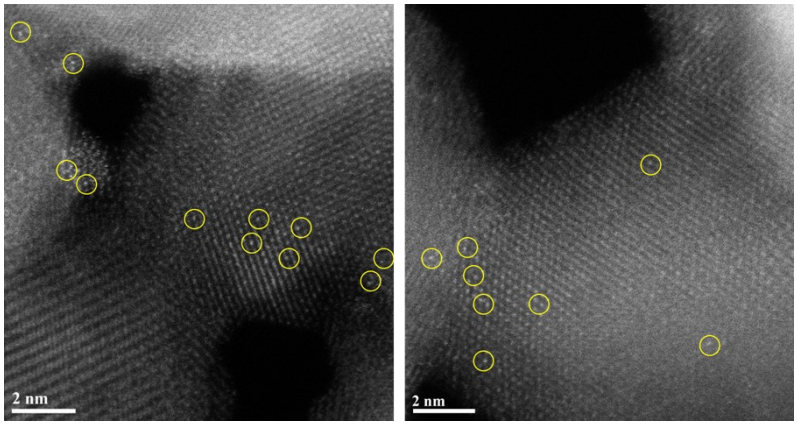

Figure S16. AC-HAADF-STEM images of the Pd/H-TiO_2 catalyst after the photothermal catalytic toluene.

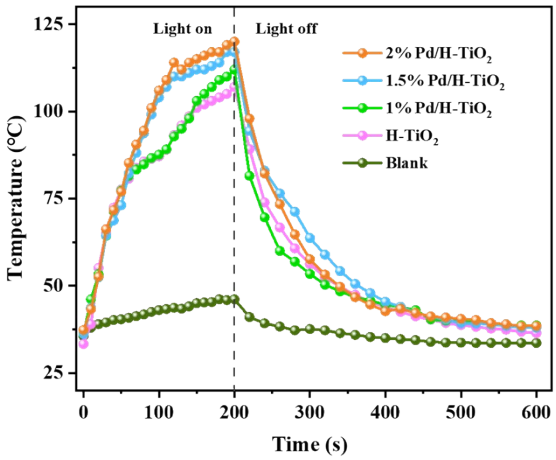

Figure S17. Surface temperature of the H-TiO_2 and Pd/H-TiO_2 samples under UV-Vis light irradiation measured by an infrared thermal imager.

The catalyst powder was loaded into a quartz reactor tube and irradiated by a 300 W xenon lamp at a lamp-to-sample distance of 10 cm. Then, thte surface temperature was monitored using an infrared thermal imaging camera after turning on the xenon lamp.

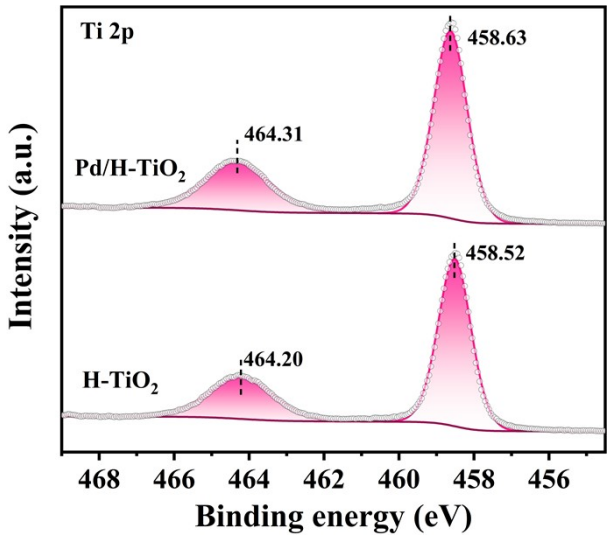

Figure S18. Ti 2p XPS spectra of H-TiO_2 and 2% Pd/H-TiO_2.

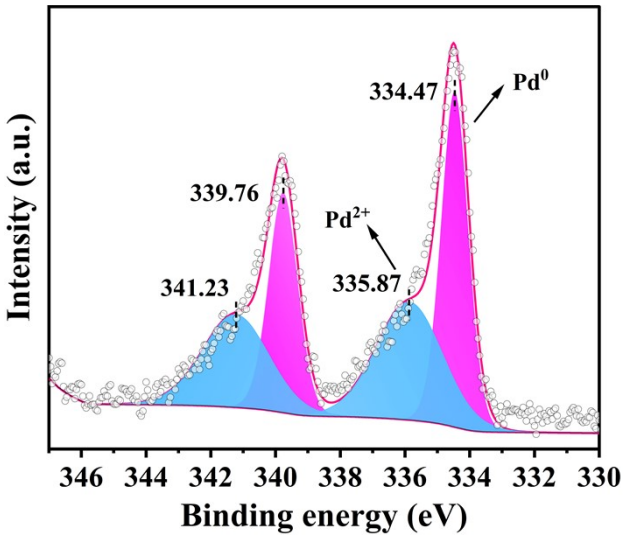

Figure S19. Pd 3d XPS spectra of 2% Pd/H-TiO_2.

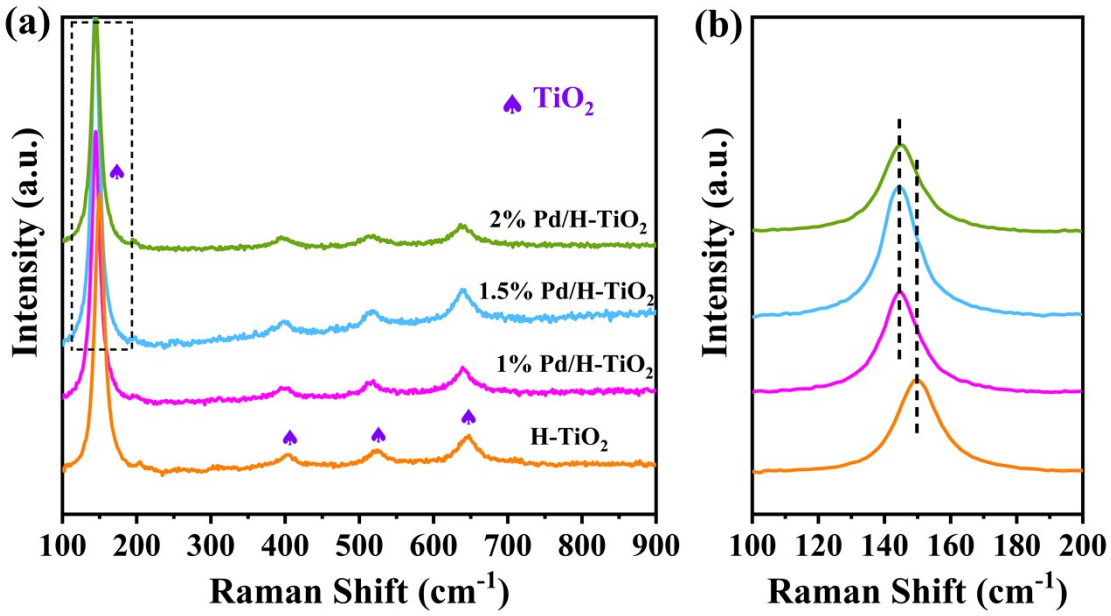

Figure S20. (a) Raman spectra of the H-TiO_2 and Pd/H-TiO_2 samples and (b) the enlarged spectra in the ranges of 100-200 cm^{-1}.

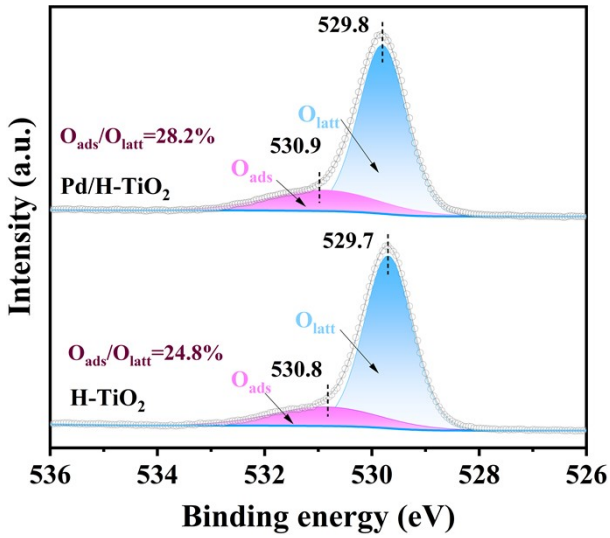

Figure S21. O 1s XPS spectra of the H-TiO_2 and Pd/H-TiO_2 catalysts.

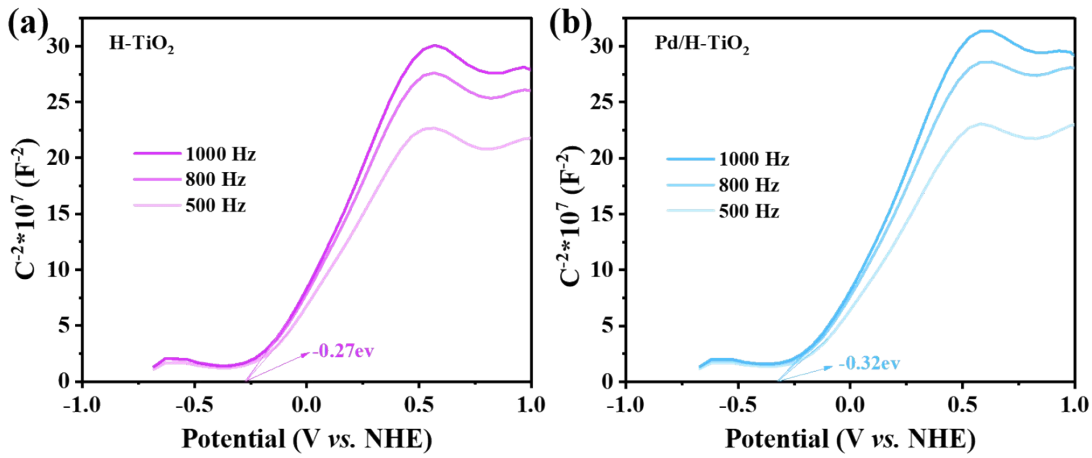

Figure S22. Mott-Schottky curves of (a) H-TiO_2 and (b) Pd/H-TiO_2 measured at 500, 800 and 1000 Hz.

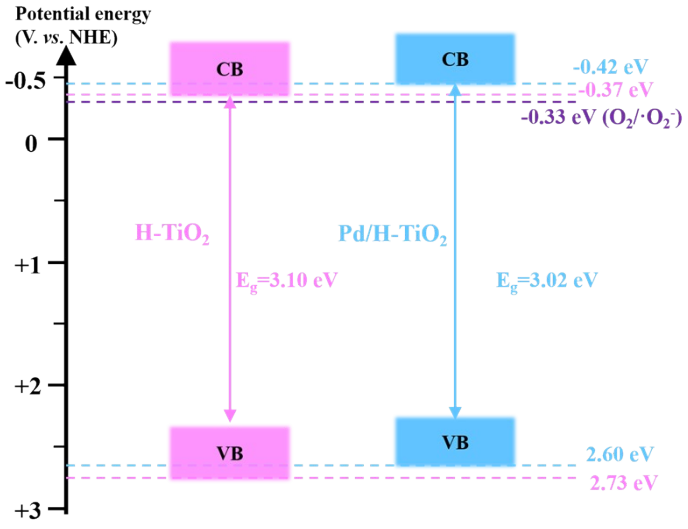

Figure S23. Band structure of H-TiO_2 and Pd/H-TiO_2.

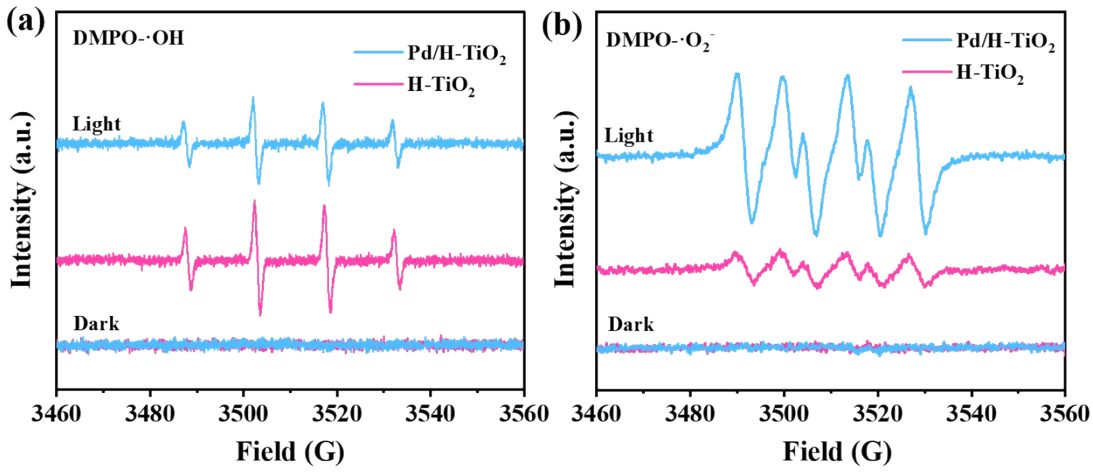

Figure S24. (a) DMPO-•OH and (b) DMPO- $^{\bullet}O_2^-$ EPR spectra of H-TiO_2, Pd/H-TiO_2 in the dark and UV-Vis light irradiation.

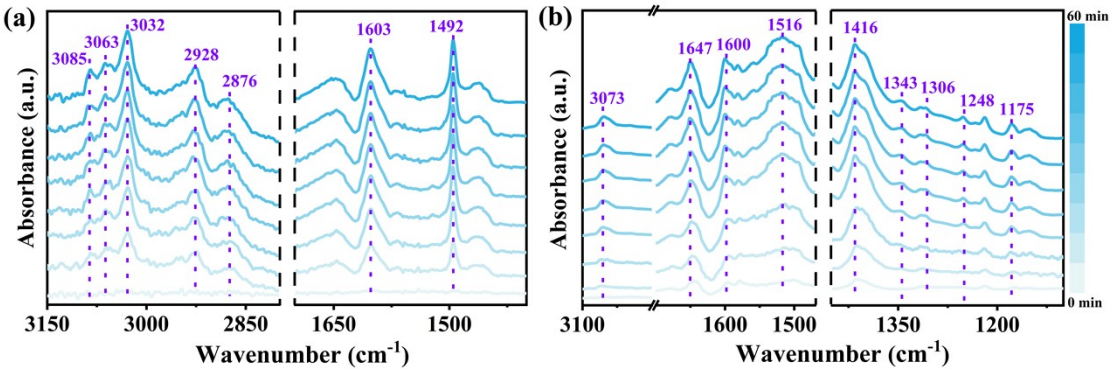

Figure S25. *In situ* DRIFT spectra of toluene adsorption (a) and oxidation (b) over Pd/H-TiO_2.

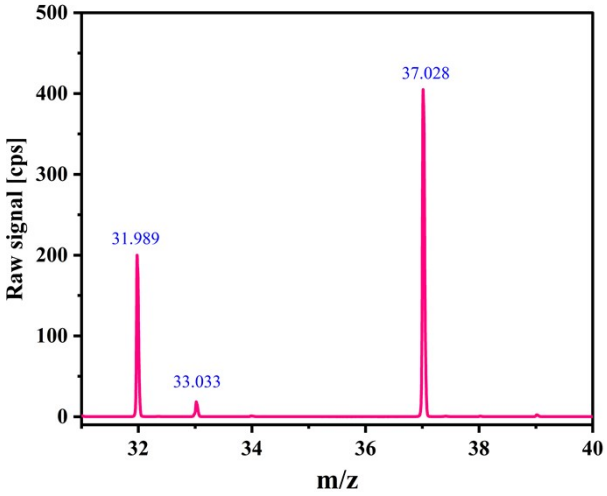

Figure S26. The possible intermediates during photothermal catalytic oxidation of toluene measured by PTR-ToF-MS.

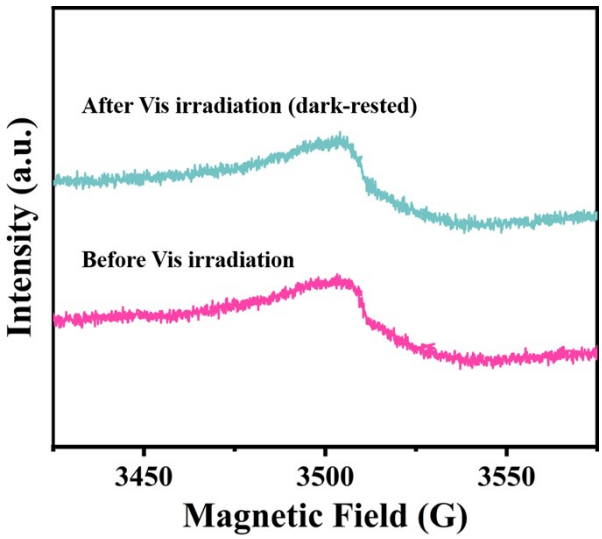

Figure S27. Solid-state EPR of Pd/H-TiO_2 before visible-light irradiation and after irradiation followed by resting in the dark for a certain period.

The reversibility of oxygen vacancies was examined by EPR spectra recorded for Pd/H-TiO_2 before visible-light irradiation and after irradiation followed by a period of

recovery in the dark (Figure S27). The results showed that the intensity of oxygen vacancies after vis light irradiation and subsequent dark storage recovered to its original level before irradiation, indicating the reversibility of the oxygen vacancies induced by vis light irradiation.

Table S1. Catalytic performance for toluene oxidation over various catalysts.

Catalyst	Toluene concentration (ppm)	GHSV (mL/g/h)	Temperature (℃)	Conversion	References
Pt/MO	200	30000	142	90%	3
0.7wt%Pd/0.4wt%Fe-TiO_2	200	30000	165	90%	4
0.5wt%Pt/Fe_2O_3	200	20000	190	90%	5
CoTi	200	30000	200	90%	6
Pt_1/CuO-CeO_2	200	20000	186	90%	7
0.65Pt/Mn- TiO_2	200	56250	197	90.4%	8
Pt-rGO-TiO_2	930	31080	176	98%	9
ZMO-H	200	30000	158	93%	10
CeO_2/$LaMnO_3$	200	31320	275	89%	11
$La_{0.9}Fe_{0.1}MnO_3$	500	30000	183	86.7%	12
Pd/H-TiO_2	200	32730	130	97%	**This work**

Table S2. Regressed reaction rate constants (k) and R^2 values for CO_2 mineralization over Pd/H-TiO_2 under UV and visible photothermal catalytic conditions.

Pd/H-TiO_2	UV	Vis
K (10^{-3} min^{-1})	2.9	29.5
R^2	0.96	0.92

Table S3. Fitted parameters for time-resolved photoluminescence tests of H-TiO_2 and Pd/H-TiO_2.

Sample		Value/ps	A		Value/μs	Rel%	Average value/ps
H-TiO_2	τ_1	126.09	8.49	B_1	25.06	17.95	215.09
	τ_2	11.33		B_2	701.10	82.05	
Pd/H-TiO_2	τ_1	151.43	10.14	B_1	22.62	18.02	240.85
	τ_2	11.19		B_2	621.56	81.98	

Reference

1. Hou, Z.; Dai, L.; Deng, J.; Zhao, G.; Jing, L.; Wang, Y.; Yu, X.; Gao, R.; Tian, X.; Dai, H.; Wang, D.; Liu, Y., Electronically Engineering Water Resistance in Methane Combustion with an Atomically Dispersed Tungsten on PdO Catalyst. *Angew. Chem., Int. Ed.* **2022,** *61*, e202201655.
2. Yu, X.; Dai, L.; Deng, J.; Liu, Y.; Jing, L.; Zhang, X.; Gao, R.; Hou, Z.; Wei, L.; Dai, H., An isotopic strategy to investigate the role of water vapor in the oxidation of 1,2-dichloroethane over the Ru/WO_3 or Ru/TiO_2 catalyst. *Appl. Catal., B* **2022,** *305*, 121037.
3. Yu, E.; Li, J.; Chen, J.; Chen, J.; Hong, Z.; Jia, H., Enhanced photothermal catalytic degradation of toluene by loading Pt nanoparticles on manganese oxide: Photoactivation of lattice oxygen. *J. Hazard. Mater.* **2020,** *388*, 121800.
4. Fan, S.; Luo, S.; Wang, Y.; Yue, X.; Zheng, D.; Zhang, Z.; Fu, X.; Dai, W., TiO_2-based Pd/Fe bimetallic modification for the efficient photothermal catalytic degradation of toluene: The synergistic effect of $\cdot O_2^-$ and ·OH species. *Sep. Purif. Technol.* **2024,** *336*, 126256.
5. Wang, Z.; Xie, S.; Feng, Y.; Ma, P.; Zheng, K.; Duan, E.; Liu, Y.; Dai, H.; Deng, J., Simulated solar light driven photothermal catalytic purification of toluene over iron oxide supported single atom Pt catalyst. *Appl. Catal., B* **2021,** *298*, 120612.
6. Yang, Y.; Zhao, S.; Bi, F.; Chen, J.; Wang, Y.; Cui, L.; Xu, J.; Zhang, X., Highly efficient photothermal catalysis of toluene over Co_3O_4/TiO_2 p-n heterojunction: The crucial roles of interface defects and band structure. *Appl. Catal., B* **2022,** *315*,

121550.

7. Feng, Y.; Dai, L.; Wang, Z.; Peng, Y.; Duan, E.; Liu, Y.; Jing, L.; Wang, X.; Rastegarpanah, A.; Dai, H.; Deng, J., Photothermal Synergistic Effect of Pt_1/CuO-CeO_2 Single-Atom Catalysts Significantly Improving Toluene Removal. *Environ. Sci.Technol.* **2022,** *56*, 8722-8732.
8. Li, G.; Zhang, M.; Chen, J.; Li, Q.; Jia, H., Combined effects of Pt nanoparticles and oxygen vacancies to promote photothermal catalytic degradation of toluene. *J. Hazard. Mater.* **2023,** *449*, 131041.
9. Li, J.-J.; Cai, S.-C.; Chen, X.; Yan, D.-X.; Chen, J.; Jia, H.-P., Engineering rGO nanosheets-adsorption layer supported Pt nanoparticles to enhance photo-thermal catalytic activity under light irradiation. *J. Mater. Chem. A* **2019,** *7*, 11985-11995.
10. Cheng, Q.; Li, Y.; Wang, Z.; Wang, X.; Zhang, G., Boosting full-spectrum light driven surface lattice oxygen activation of $ZnMn_2O_4$ by facet engineering for highly efficient photothermal mineralization of toluene. *Appl. Catal., B* **2023,** *324*, 122274.
11. Li, J.-J.; Yu, E.-Q.; Cai, S.-C.; Chen, X.; Chen, J.; Jia, H.-P.; Xu, Y.-J., Noble metal free, CeO_2/$LaMnO_3$ hybrid achieving efficient photo-thermal catalytic decomposition of volatile organic compounds under IR light. *Appl. Catal., B* **2019,** *240*, 141-152.
12. Yu, Q.; Li, C.; Zhao, J.; Liu, X.; Huang, L.; Zhu, Y.; Yang, K.; Zhang, Z.; Ma, D.; Zhang, Y.; Huang, Q., Efficient photothermal catalytic oxidation of toluene by $La_{1-x}Fe_xMnO_3$ with full spectrum response: The effects of Fe doping and photoactivation. *Appl. Catal., B* **2023,** *327*, 122441.